GeoExpert ag

swiss*nuclear*: PEGASOS Refinement Project:
SP2 – Ground Motion Characterization

Contract no. PMT-VT-1032

Seismic Shear Wave Velocity Determination and Hybrid Seismic Survey at the SED-Station WIMIS (Wimmis, BE)

Date of Field Data Acquisition 24th April 2009

Report

Client

swiss*nuclear*
Project PRP
Frohburgstrasse 17
4601 Olten

Contractor

GeoExpert ag
Seismic Prospecting
Ifangstrasse 12b
P.O. Box 451
8603 Schwerzenbach

8603 Schwerzenbach, 9th July 2009

INDEX

1 INTRODUCTION

1.1 Survey objectives

The seismic survey's main task is to provide information about the distribution function of the shear wave velocities in the depth interval of the uppermost 30 m along a 100 m long seismic profile.

Additionally, the following objectives are to be met:

- the mapping of the topography of the rock face, i.e. the thickness of the Quaternary deposits;
- the determination of the thickness of the weathered zone and its degree of decompaction at the bedrock surface;
- a general view of geological structures.

1.2 The choice of the appropriate surveying methods

Several methods are available for deriving the s-wave velocity distribution in the subsurface at any given position:

- in-situ measurement by down-hole or crosshole seismic surveying;
- shear-wave refraction tomography profiling;
- dispersion analysis of surface waves (MASW; **M**ultiple channel **A**nalysis of **S**urface **W**aves)

The surveys are to be carried out at, or as close as possible near some 20 SED earth quake monitoring stations in Switzerland. Ideally, the surveys are to be conducted on two orthogonal profiles in order to derive at their point of intersection a robust 1D s-wave velocity distribution function by correlation. To this end, the methods of MASW and shear-wave refraction tomography profiling are to be combined.

The results are to include the following fundamental parameters $v_{s,5}$, $v_{s,10}$, $v_{s,20}$, $v_{s,30}$, $v_{s,40}$, $v_{s,50}$, $v_{s,100}$ are to be calculated, also an error estimation of all values.

The data acquired for the MASW method are to be subjected to complementary **p-wave hybrid seismic data processing** in order to image the geological structures.

2 FIELD DATA ACQUISITION PARTICULARS

2.1 Time Schedule

Date	*Time*	*Activities / remarks*
23.04.2009	1535	arrival at site
	1535 - 1630	site reconnaissance and discussion with SED about array layouts
	1630	leaving from site
24.04.2009	0800	arrival at site
	0800 - 0815	site reconnaissance
	0815 - 0915	lay-out of spread profile 1 (p-wave and s-wave)
	0915 - 1015	data acquisition of spread profile 1 (p-wave)
		data acquisition of spread profile 1 (s-wave)
	1015 - 1200	lay-out of spread profile 2 (p-wave and s-wave)
	1310 - 1440	data acquisition of spread profile 2 (p-wave)
		data acquisition of spread profile 2 (s-wave)
	1440 - 1500	removal of the seismic measuring system
	1500 - 1715	departure from site

2.2 Summary of Data Acquisition Parameters

Compressional Wave Data Acquisition

# of active channels	96
geophone type	4.5 Hz natural frequency, vertical velocimeter
receiver station spacing	1.0 m
# of geophones/station	1
source point spacing	2.0 m to 3.0 m
source type	vertical hammer (8 kg) striking on a horizontal metal plate
sampling rate	500 µs
recording time	2048 ms
field filters	0.5 Hz LC, anti-alias
# of field records	27 (line 09SN_20WIMIS-P1) and 27 (line 09SN_20WIMIS-P2)

Shear Wave Data Acquisition

# of active channels	48
geophone type	10 Hz natural frequency, horizontal velocimeter
receiver station spacing	2.0 m
# of geophones/station	1
source point spacing	4.0 m to 6.0 m
source type	horizontal hammer (8 kg) striking horizontally at a metal-plated wooden beam anchored to the ground by means of 20 cm long spikes
sampling rate	500 µs
recording time	512 ms
field filters	2 Hz LC, anti-alias
# of field records	30 (line 09SN_20WIMIS-S1) and 45 (line 09SN_20WIMIS-S2)

Fig. 2.1: S-wave data acquisition at profile 09SN_20WIMIS-S2 with a small motorized wheel barrow to transport the shear wave generator to the site in difficult areas.

2.3 Composition of Seismic Field Crew

Personnel

Lorenz Keller	dipl.-Natw. ETH, geophysicist, party chief
Dieter Martin	dipl.-Geol., University of Freiburg i. Br., geologist, party chief
Jochen Fiseli	dipl.-Geol., University of Freiburg i. Br., geologist, spread lay-out and activation of seismic source

Equipment

96	vertical geophones 4.5 Hz
48	horizontal geophones 12 Hz
6	seismic cables
1	seismic acquisition system Summit Compact, 96 channels
1	laptop computer for data acquisition
3	walkie-talkies
1	hammer 8 kg
1	steel plate
1	metal-plated wooden beam
1	van (FIAT Ducato 4x4)

2.4 Location

The seismic monitoring station WIMIS (Wimmis, BE, Swiss prealps) is situated in a massive formation of Jurassic limestones (Malmkalk), encircled by a complex geological setting with Quaternary deposits.

Fig. 2.2: The red cross marked seismic monitoring station WIMIS (Wimmis, BE) is located in Jurassic sediments (Malmkalk). (map: geodata @ swisstopo).

2.5 Recording Conditions and Line Setup

Warm temperatures prevailed throughout the field data recording period.

In general, the data quality obtained at WIMIS is to be rated as fair.

Due to the difficulties in acquisition geometry, it was decided on site to lay out the arrays along two different areas where the limestone cliff dips vertical into the Quaternary deposits. Measurements above the cliff (Burgstock) were impracticable because of logistical matters and on the Quaternary deposits (Burgmatte/Spissiweid) wouldn't be able to allow velocity determination of the bedrock. So, one profile was positioned directly along the entrance to the military bunker, the second one 350 m to the West.

2.6 Seismic Wave Generation

Due to the geological setting – vertical separated limestone and soft rock – and the impossibility to generate shear waves on the hard rock with the shear wave beam, we decided in agreement with the SED to generate both compressional and shear waves directly by hitting the hard rock in the respective directions.

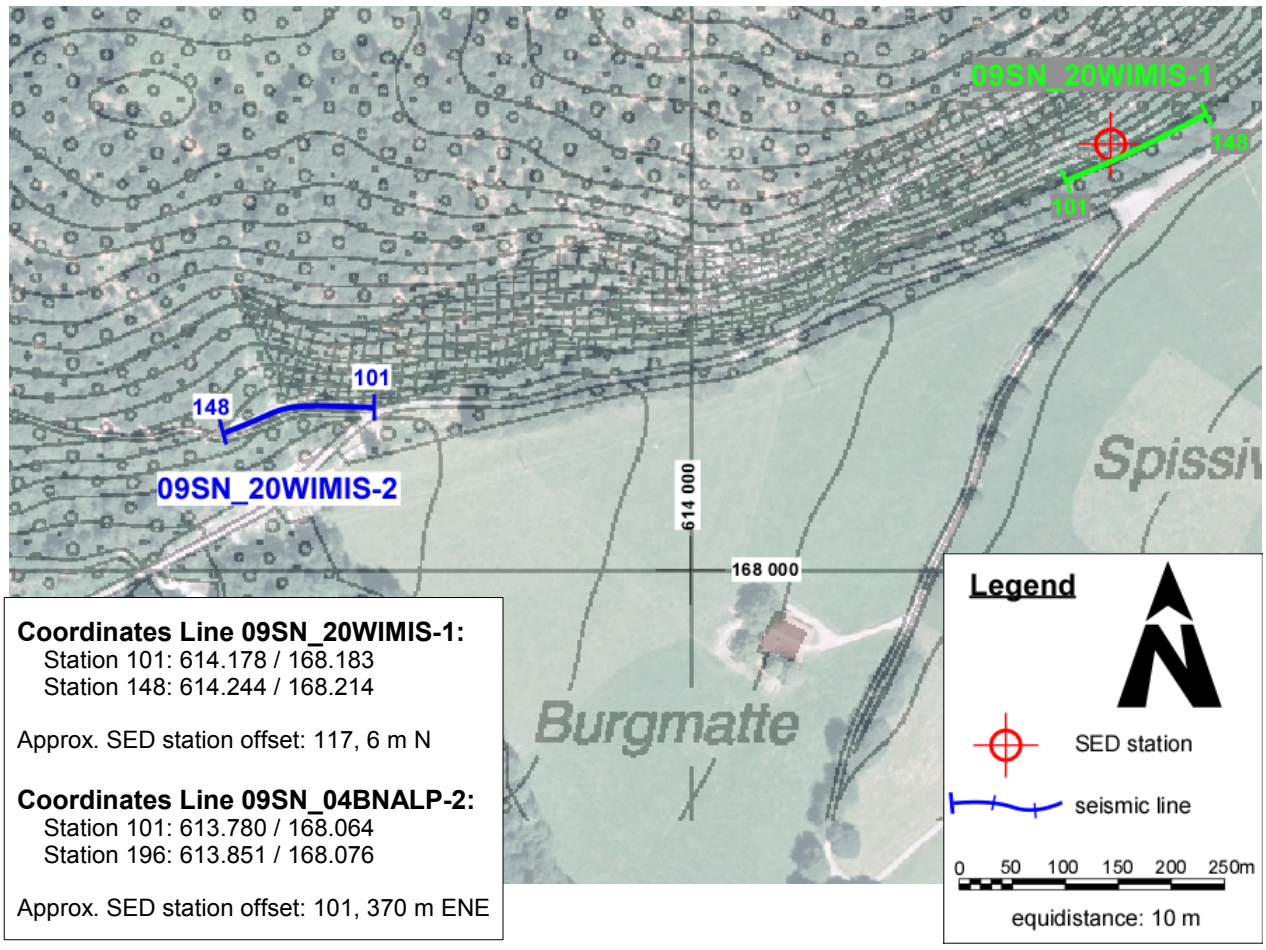

Fig. 2.3: Situation map with the trace of seismic profile 09SN_20WIMIS-1 and -2. (background map: © Amt für Geoinformation des Kantons Bern und SWISSIMAGE © swisstopo (DV043667.1))

3 SEISMIC DATA PROCESSING AND IMAGING OF THE RESULTS

3.1 General Remarks

- For the shear and compressional wave refraction seismic evaluation the package **RAYFRACT** by Intelligent Resources Ltd., Vancouver CAN, was used. The system features the technique of diving wave tomography (www.rayfract.com).
- The system **SPW** (**S**eismic **P**rocessing **W**orkshop) of Parallel Geoscience Corporation, Austin US-TX, was used for reflection seismic data processing (www.parallelgeo.com).
- Data processing of surface waves (MASW processing) was conducted with the software package **SurfSeis** V2.0 of Kansas Geological Survey in Lawrence US-KS.

A detailed description of the various surveying methods will be included in the general summary report.

3.2 Shear Wave Refraction Tomography

3.2.1 Reformatting and field geometry assignment

After reformatting the field data into the Rayfract format the field geometry is applied.

3.2.2 First break time picking

At each shot position, two seismic records were acquired in both activation directions. These two records are displayed superimposed with different colors on each other in Fig 3.2a together with the manually determined first arrival time picks.

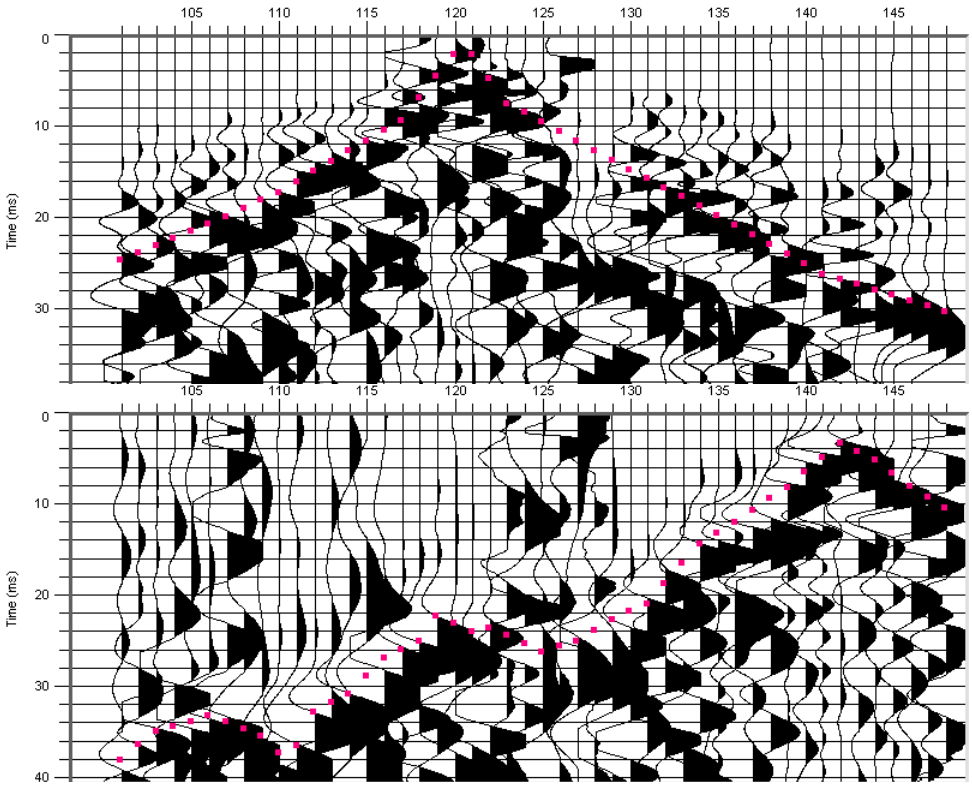

Fig. 3.2a: Record of line 09SN_20WIMIS-S1 (top) and -S2 (bottom) showing at each station the s-wave traces. The manually picked s-wave refraction arrivals at each station are marked with an red square. The station spacing is 1.5 m.

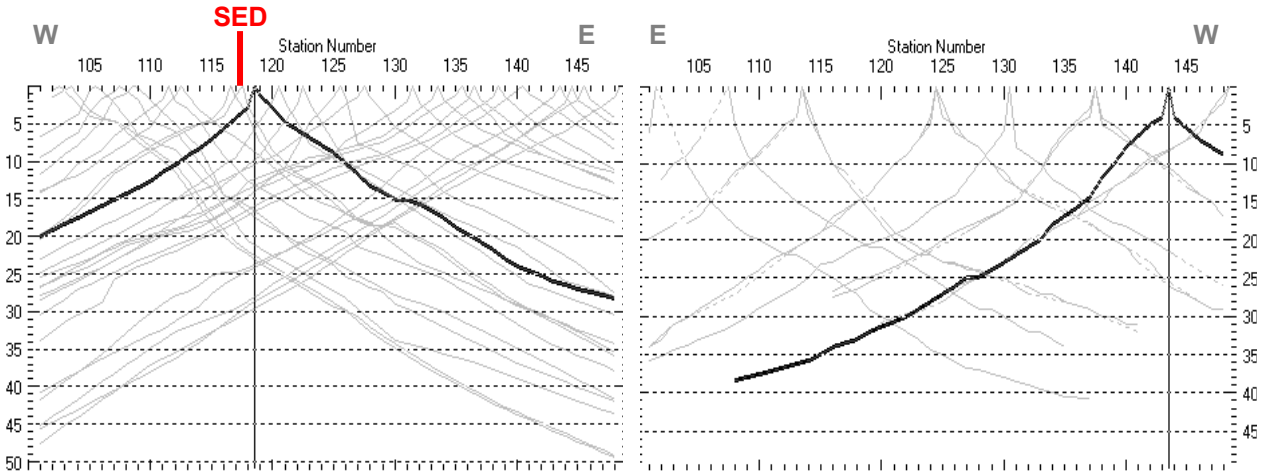

Fig. 3.2b: Curves of s-wave first break time picks of line 09SN_20WIMIS-S1 (left) and -S2 (right). Station number 101 = profile meter 0; station number 148 = profile meter 72. Station spacing is 1.5 m.

3.2.3 Analytical Determination of Refraction Velocities

An initial 1D-velocity function (averaged 1D velocity-depth profiles derived by the Delta-t-V method, see Tab. 3.2a) is determined in the 3-dimensional time-offset-CMP-domain of all first break arrival time curves in the 3-dimensional time-offset-CMP-domain (see. Fig. 3.2c).

Depth [m]	Vs [m/s]
0.0	792
0.3	864
0.5	951
0.9	1090
1.3	1193
2.0	1350
2.8	1496
4.0	1564
5.5	1658
7.6	1754
10.3	1696
14.1	1746
19.2	1903
26.0	2581

Depth [m]	Vs [m/s]
0.0	319
0.4	597
0.7	715
1.1	853
1.6	953
2.5	1083
3.6	1243
5.2	1521
7.4	1815
10.6	1792
15.0	1770
21.1	2746
29.8	4882

Tab. 3.2a: Initial 1D s-wave velocity function derived from real data of line 09SN_20WIMIS-S1 (horizontal mean values) and of line -S2 (horizontal mean values).

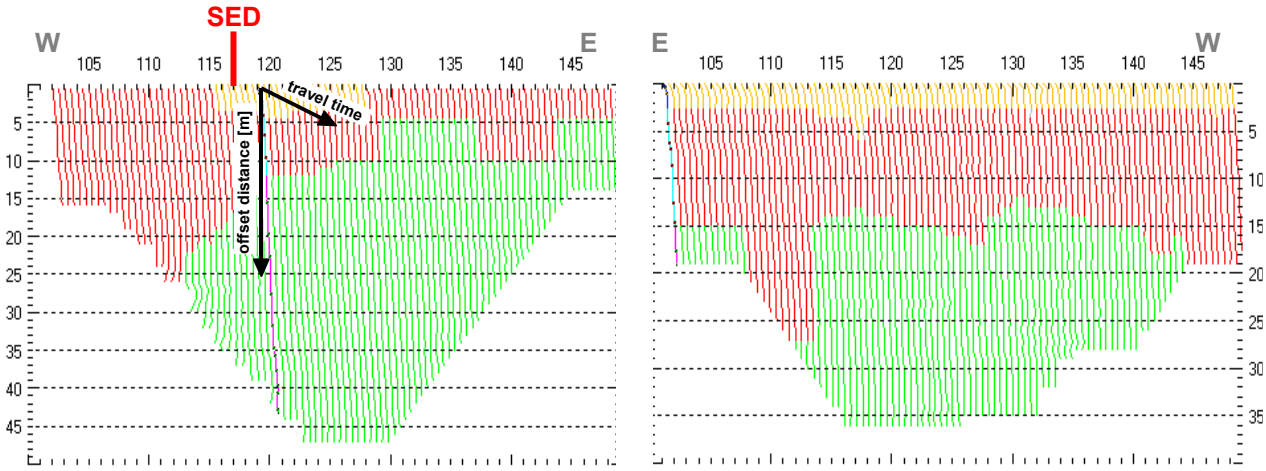

Fig. 3.2c: 3-dimensional distance-travel time diagrams of line 09SN_20WIMIS-S1 (left) and 09SN_20WIMIS-S2 (right) at the mid-points between source points and receiver stations are instrumental when using the analytical CMP derivation of the initial velocity field.
The horizontal axes are the along the CMP positions and the travel time respectively, the vertical axis denotes the offset distance between source and receiver positions. The colors represent different velocity layers. The station spacing is 2 m, profile station number 00 = profile meter 0; profile station number 48 = profile meter 96. The colors represent different velocity layers.

3.2.4 Tomographic inversion of the velocity gradient field by iterative modeling

The velocity field is iteratively refined by the subsequent Wavepath Eikonal Traveltime (WET) tomographic inversion process. The inversion results are portrayed in Fig. 3.2d as a gridded velocity contour section and in Fig. 3.2e as a ray path density section.

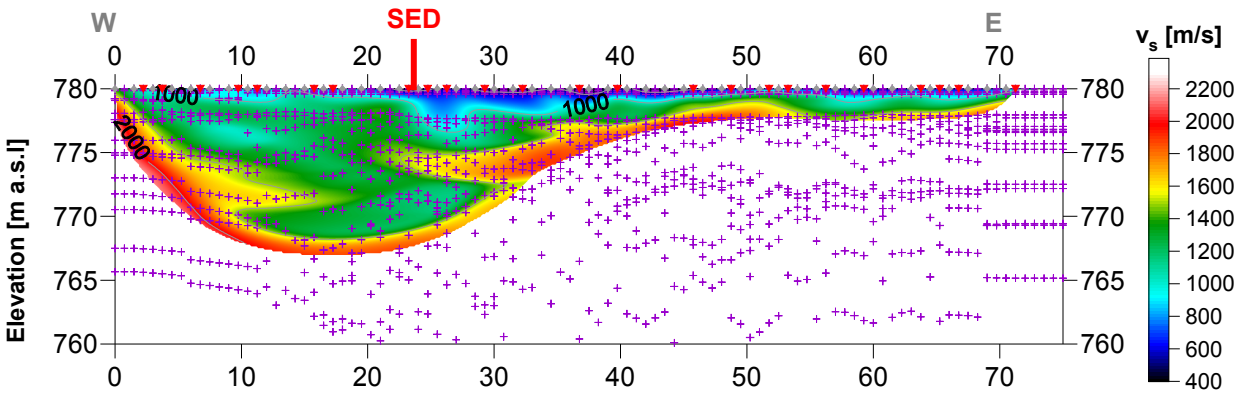

Fig. 3.2d: Shear wave velocity field of the line 09SN_20WIMIS-S1. Red/white colors denote solid rock, blue/black colors point to unconsolidated sediments and soil.
Vertical axis: elevation [m a.s.l]; horizontal axis: profile meter; color encoded scale: v_s [m/s]; no vertical exaggeration; gray diamonds: receiver positions; red triangles: source positions; magenta crosses: positions of determined velocity values. The station spacing is 2 m, profile meter 0 = profile station number 00, profile meter 96 = profile station number 48.

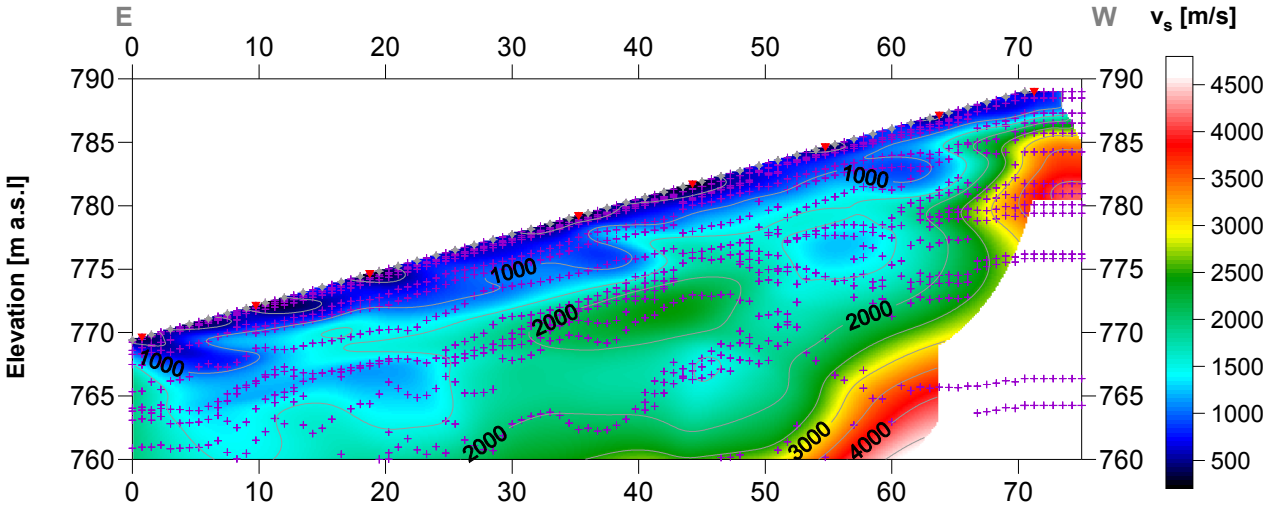

Fig. 3.2e: Shear wave velocity field of the line 09SN_20WIMIS-S2. Red/white colors denote solid rock, blue/black colors point to unconsolidated sediments and soil. Vertical axis: elevation [m a.s.l]; horizontal axis: profile meter; color encoded scale: v_s [m/s]; no vertical exaggeration; gray diamonds: receiver positions; red triangles: source positions; magenta crosses: positions of determined velocity values. The station spacing is 1.5 m, profile meter 0 = profile station number 101, profile meter 72 = profile station number 148.

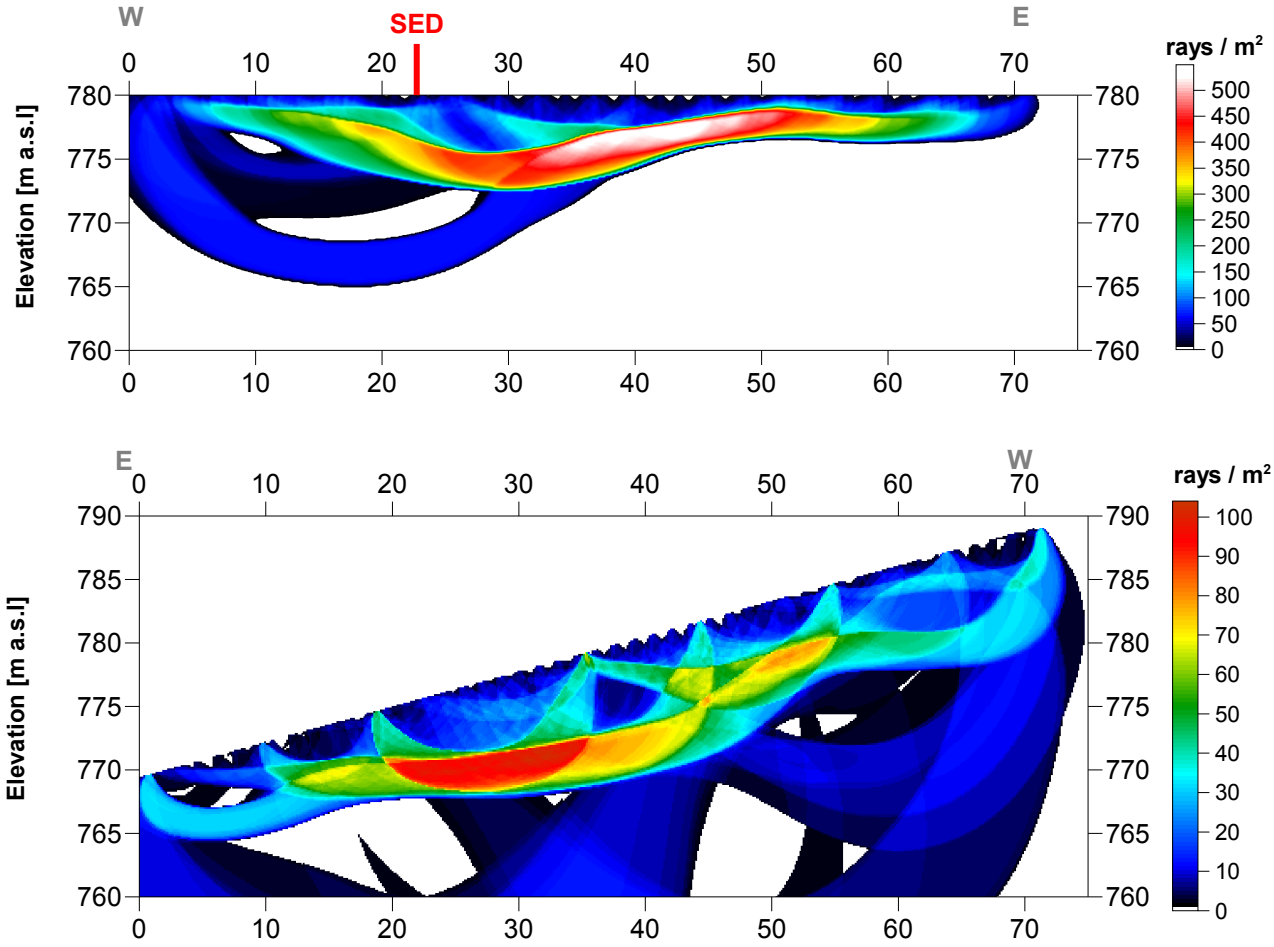

Fig. 3.2f: Shear wave ray path density along the seismic line 09SN_20WIMIS-S1 (top) and -S2 (bottom). Red/white colors indicate high velocity contrasts (usually at the bedrock surface), blue/black colors denote low coverage areas. Vertical axis: elevation [m a.s.l]; horizontal axis: profile meter; color encoded scale: ray paths per m²; no vertical exaggeration. The station spacing is 1.5 m, profile meter 0 = profile station number 101, profile meter 72 = profile station number 148.

Depth [m]	Vs [m/s]
0.0	695
0.8	1050
1.6	1286
2.4	1373
3.2	1349
4.0	1380
4.8	1496
5.6	1548
6.4	1570
7.2	1498
8.0	1487
8.8	1485
9.6	1438
10.4	1427
11.2	1504
12.0	1768
12.8	1878

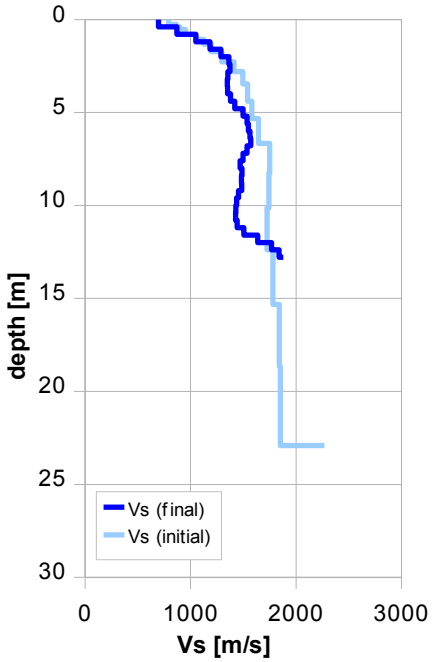

Tab. 3.2b: Final 1D s-wave velocity model derived from real data of line 09SN_20WIMIS-S1 (horizontal average of all values). The calculated values of the initial 1D s-wave velocity model are given in Tab. 3.2a.

Depth [m]	Vs [m/s]
0.0	536
1.2	764
2.4	1121
3.6	1359
4.8	1518
6.0	1695
7.2	1839
8.4	1926
9.6	1823
10.8	1781
12.0	1770
13.0	1790
14.2	1861
15.4	1971
16.6	2109
17.8	2256
19.0	2447

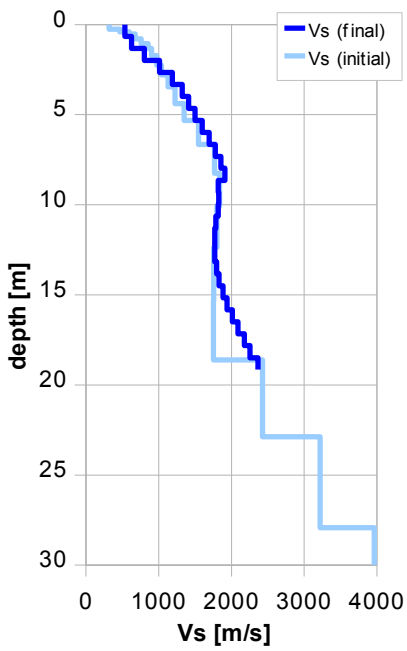

Tab. 3.2c: Final 1D s-wave velocity model derived from real data of line 09SN_20WIMIS-S2 (horizontal average of all values). The calculated values of the initial 1D s-wave velocity model are given in Tab. 3.2a.

3.3 MASW Processing

3.3.1 Reformatting and field geometry assignment

The data preparation steps for the dispersion analysis include

- the assignment of the field acquisition geometry
- the selection of suitable offset ranges (=arrays) between 10 m and 50 m for dispersion, and the splitting of the field records in forward and reverse shooting direction data sets
- the reformatting of the data into the specific KGS format

X - - ... - - o-o-o-...-o-o-o (forward shooting or so-called PLUS direction)
respectively
o-o-o-...-o-o-o - - ... - - X (reverse shooting or so-called MINUS direction).

where **X** = shot position
o = receiver station
- = 1.0 m offset

The active array used at SED-station WIMIS are the receiver station in the shot offset range between 10 and 50 m.

3.3.2 Calculating the dispersion image (overtone)

The result of dispersion analysis is the color encoded acoustic energy distribution in the phase velocity - frequency plane (see Fig. 3.3a and b).

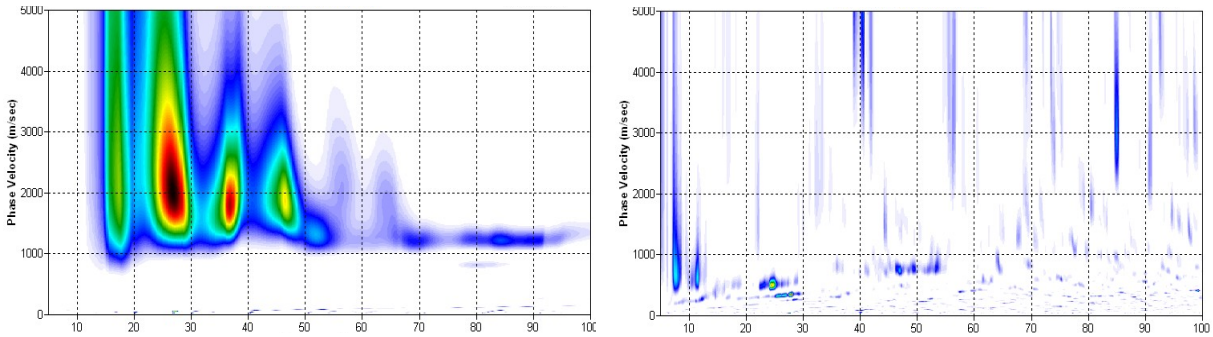

Fig. 3.3a: Dispersion image of moderat quality data (left) from line 09SN_20WIMIS-M1_MINUS as found on 30 % and of deficient quality data (right) from line 09SN_20WIMIW-M2_MINUS representing about 70 % of the MASW dataset of site WIMIS.
Horizontal axis: frequency from 5 to 100 Hz; vertical axis: phase velocity from 0 to 5000 m/s; color code: colors from white (no energy) to blue - green - yellow - red - black point to increasing energy amplitude values.

3.3.3 Analysis of the dispersion image

In the dispersion graphs as calculated in section 3.3.2 above, the curves joining the amplitude peaks of the fundamental modes are determined either by subjective inspection or in a semi-automated manner. On datasets with poorly defined amplitude peaks or with a highly irregular alignment of the peaks, the danger of obtaining improbable or wrong results is real and can only be mitigated by the processing experience and the a-priori knowledge of the geological setting by the geophysicist responsible for the data evaluation.

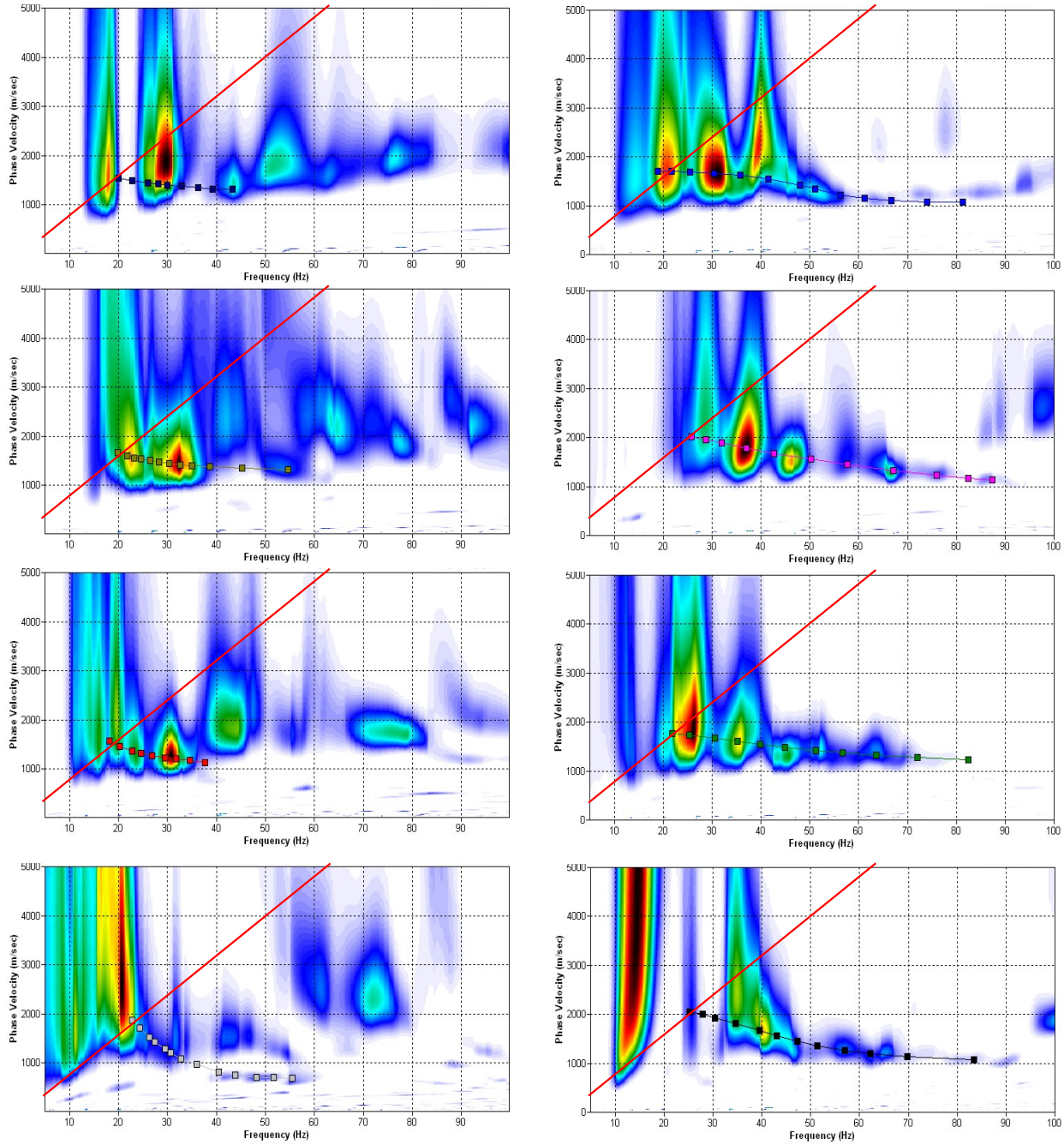

Fig. 3.3b: The manually picked dispersion images used for the derivation of the shear wave velocity section on line 09SN_20WIMIS-M1. The dispersion curves (squares) are determined by linking the peaks of high energy. Note that 'higher modes' may at times produce higher energy peaks than the fundamental mode required for the analysis.
dotted fine line: signal-noise ratio for the designated f-v_{ph} – value.
red line: high resolution beam-forming curve for v_{max}.
1st row: left: station 123 @ PLUS direction; right: station 118 @ MINUS direction
2nd row: left: station 127 @ PLUS direction; right: station 123 @ MINUS direction
3rd row: left: station 132 @ PLUS direction; right: station 125 @ MINUS direction
4th row: left: station 135 @ PLUS direction; right: station 128 @ MINUS direction

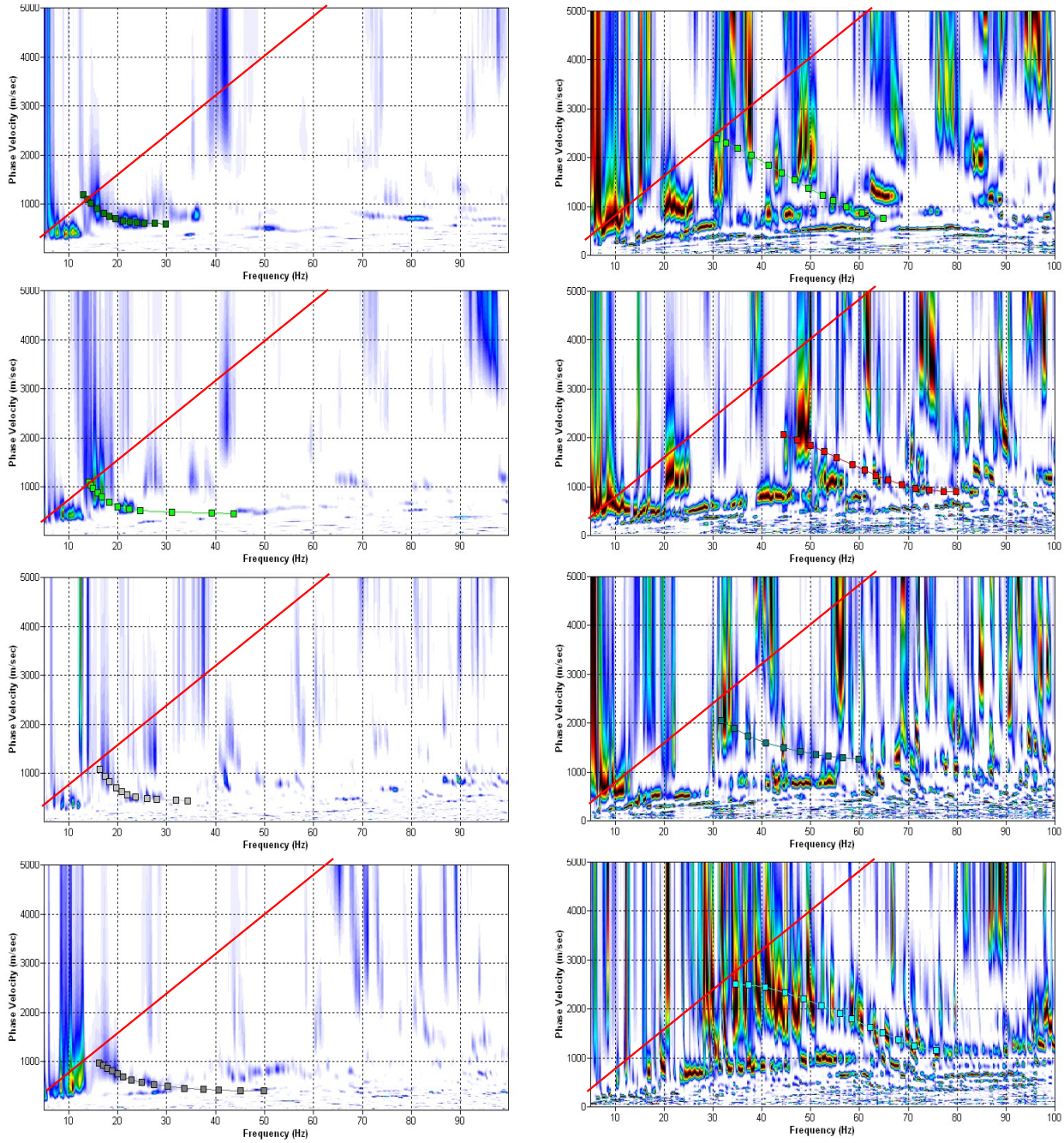

Fig. 3.3c: The manually picked dispersion images used for the derivation of the shear wave velocity section on line 09SN_20WIMIS-M2. The dispersion curves (squares) are determined by linking the peaks of high energy. Note that 'higher modes' may at times produce higher energy peaks than the fundamental mode required for the analysis.
dotted fine line: signal-noise ratio for the designated f-v_{ph} – value.
red line: high resolution beam-forming curve for v_{max}.
1st row: left: station 121 @ PLUS direction; right: station 120 @ MINUS direction
2nd row: left: station 123 @ PLUS direction; right: station 122 @ MINUS direction
3rd row: left: station 125 @ PLUS direction; right: station 124 @ MINUS direction
4th row: left: station 134 @ PLUS direction; right: station 128 @ MINUS direction
Dispersion images of MINUS-direction are vertical normalized to show any dispersion event.

3.3.4 Inversion of dispersion curves resulting in a 1D shear wave velocity distribution

Inversion of the extracted dispersion curves was performed using the algorithm described by Xia et al. (1999).

The inversion process is started by setting the maximum depth (z_{max}) to be in the order of 30% of the largest wavelength for an initial model consisting of 10 layers of increasing thicknesses. For all 10 layers the Poisson's ratio is assumed to be 0.4 and the rock/soil density to be 2.0 g/cm^3. The inversion process is concluded either after twelve iterations or when the convergence condition of a RMS-error of less than 3 m/s (phase velocity) is met.

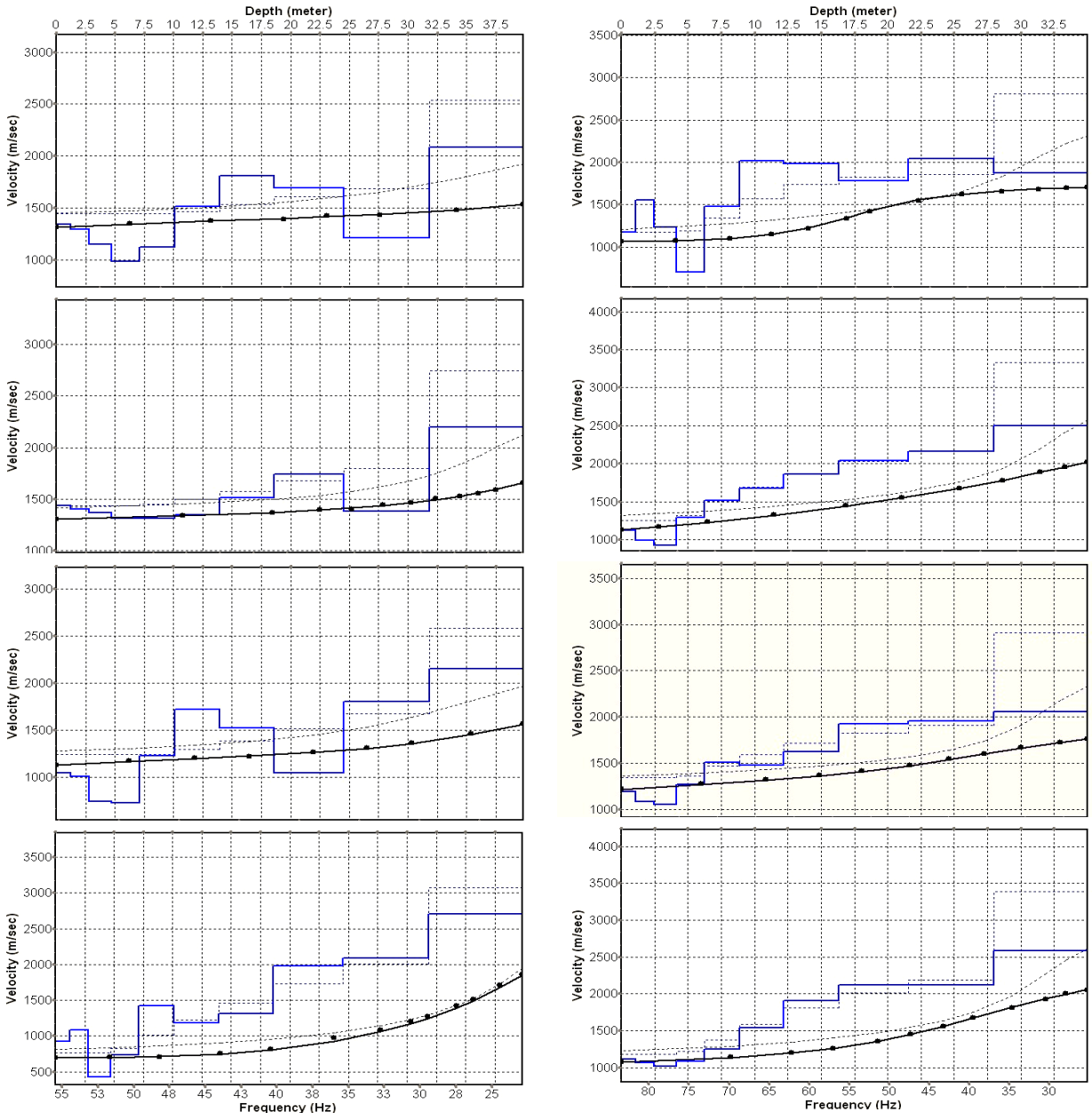

Fig. 3.3d: Inversion results of dispersion curves of dataset at line 09SN_20WIMIS-M1.
***brown**: Inversion of dispersion curve (dots) resp. of the modeled dispersion curve (dotted line: initial model; continuous line: end model). Horizontal axis: frequency Hz, vertical axis: v_s.*
***blue**: 10-layer-model (dotted: initial model, continuous line: final model). Horizontal axis: depth, vertical axis: phase velocity resp. v_S).*
1st row: left: station 123 @ PLUS direction; right: station 144 @ MINUS direction
2nd row: left: station 127 @ PLUS direction; right: station 123 @ MINUS direction
3rd row: left: station 132 @ PLUS direction; right: station 125 @ MINUS direction
4th row: left: station 135 @ PLUS direction; right: station 128 @ MINUS direction

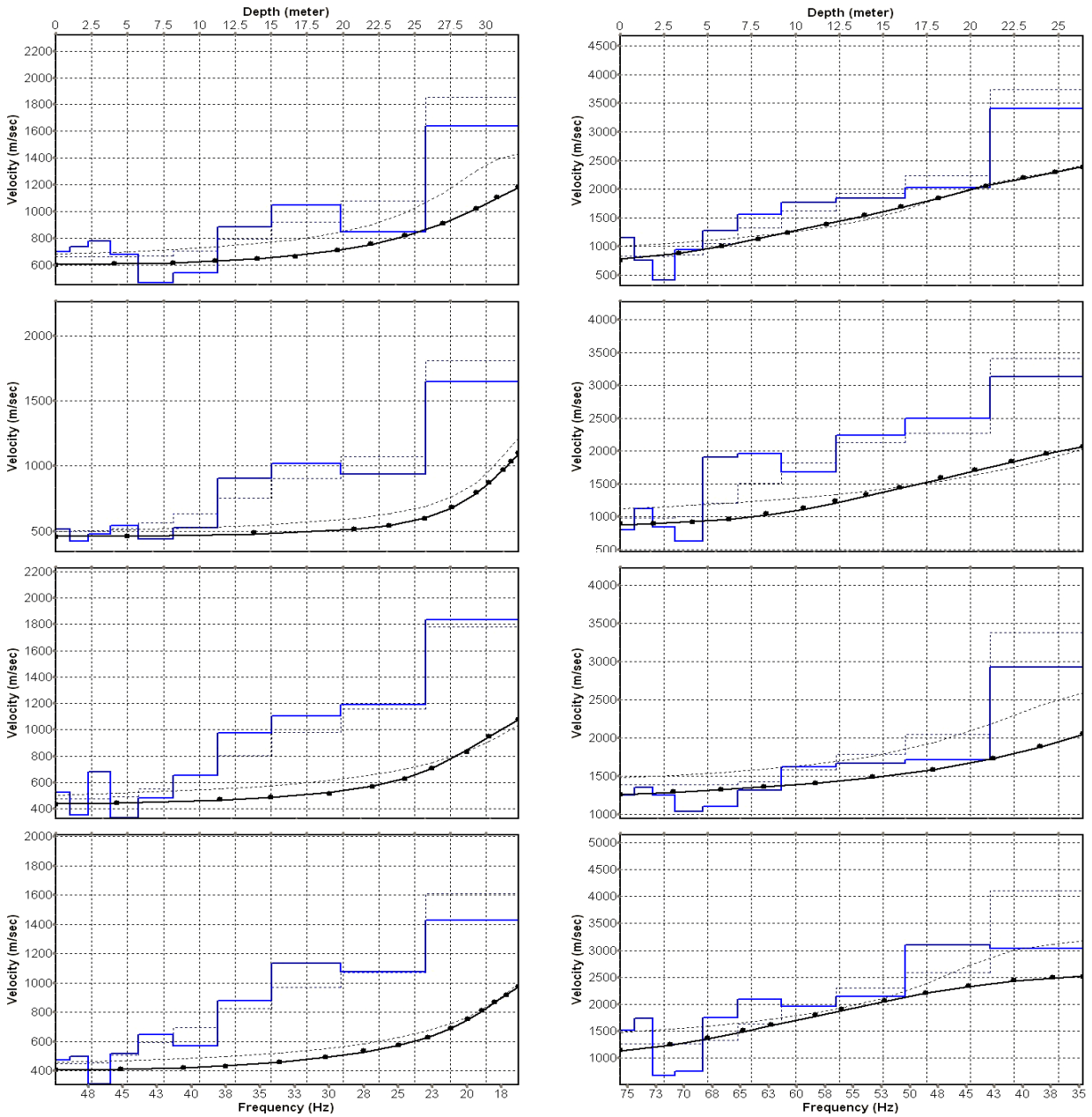

Fig. 3.3e: Inversion results of dispersion curves of dataset at line 09SN_20WIMIS-M2.
***brown**: Inversion of dispersion curve (dots) resp. of the modeled dispersion curve (dotted line: initial model; continuous line: end model). Horizontal axis: frequency Hz, vertical axis: v_s.*
***blue**: 10-layer-model (dotted: initial model, continuous line: final model). Horizontal axis: depth, vertical axis: phase velocity resp. v_s).*
1st row: left: station 28 @ PLUS direction; right: station 31 @ MINUS direction
2nd row: left: station 40 @ PLUS direction; right: station 41 @ MINUS direction
3rd row: left: station 49 @ PLUS direction; right: station 47 @ MINUS direction
4th row: left: station 58 @ PLUS direction; right: station 56 @ MINUS direction

Dispersion analyses of records with longer receiver arrays should – by theory – increase the investigation depth. At WIMIS, with both lines and both directions, MASW processing with the maximal array length of 72 m improve the results slightly (Fig. 3.3f and 3.3g).

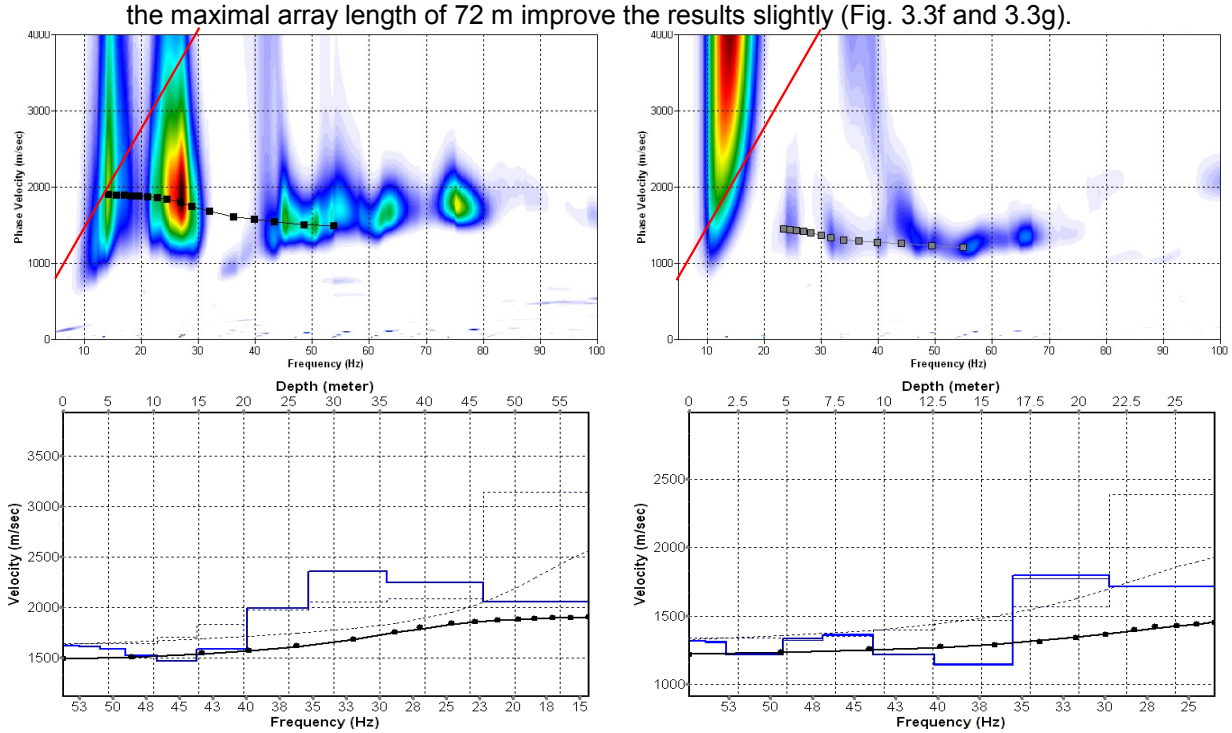

Fig. 3.3f: Top: dispersion images of over-all arrays (10...82 m offset) of line 09SN_20WIMIS-M1 in PLUS (left) and MINUS (right) direction; dotted fine line: signal-noise ratio for the designated f-v_{ph}-value. Red line: high resolution beam-forming curve for v_{max}.
*Below: The two respective inversion results; **brown**: inversion of dispersion curve; **blue**: 10-layer-model. Horizontal axis: depth, vertical axis: phase velocity resp. v_s.*

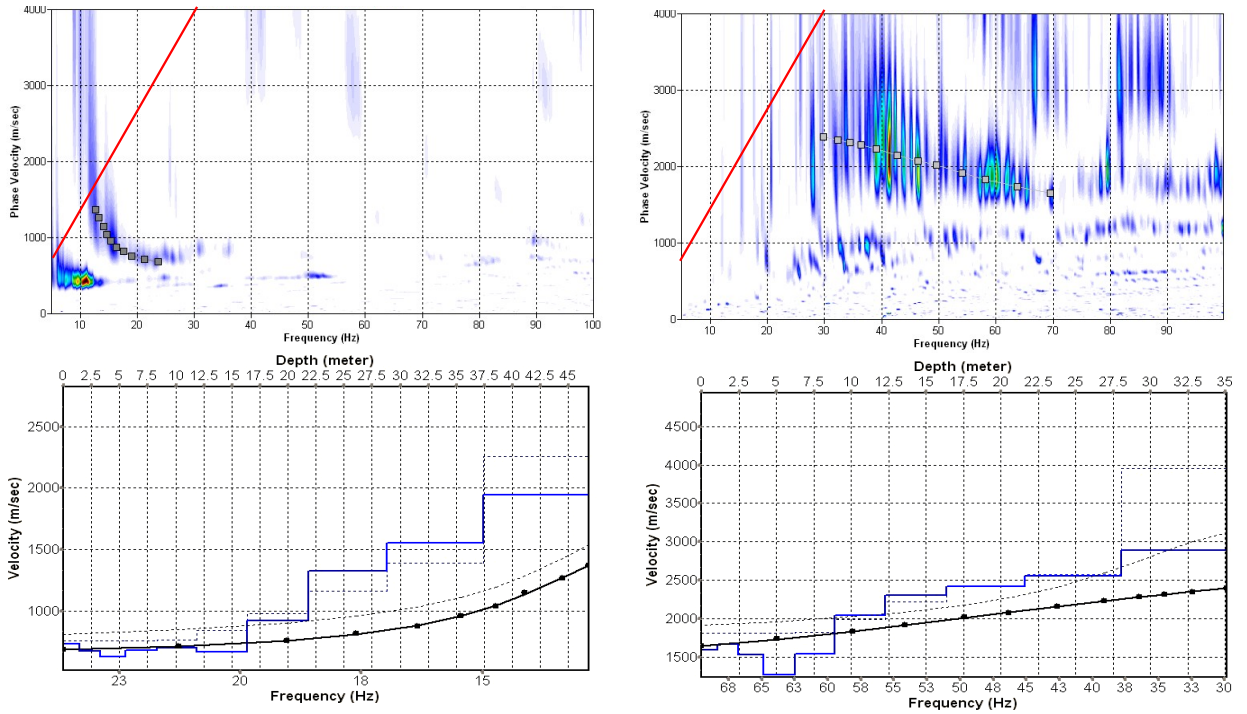

Fig. 3.3g: Top: dispersion images of over-all arrays (10...82 m offset) of line 09SN_20WIMIS-M2 in PLUS (left) and MINUS (right) direction; dotted fine line: signal-noise ratio for the designated f-v_{ph} – value. Red line: high resolution beam-forming curve for v_{max}.
*Below: The two respective inversion results; **brown**: inversion of dispersion curve; **blue**: 10-layer-model. Horizontal axis: depth, vertical axis: phase velocity resp. v_s.*

3.3.5 Gridding and plotting of 2D v_s-velocity field

By assembling the 1D v_s - depth functions of all stations the final 2D v_s-field is derived using a Kriging gridding procedure as portrayed in Fig. 3.3h and 3.3i below:

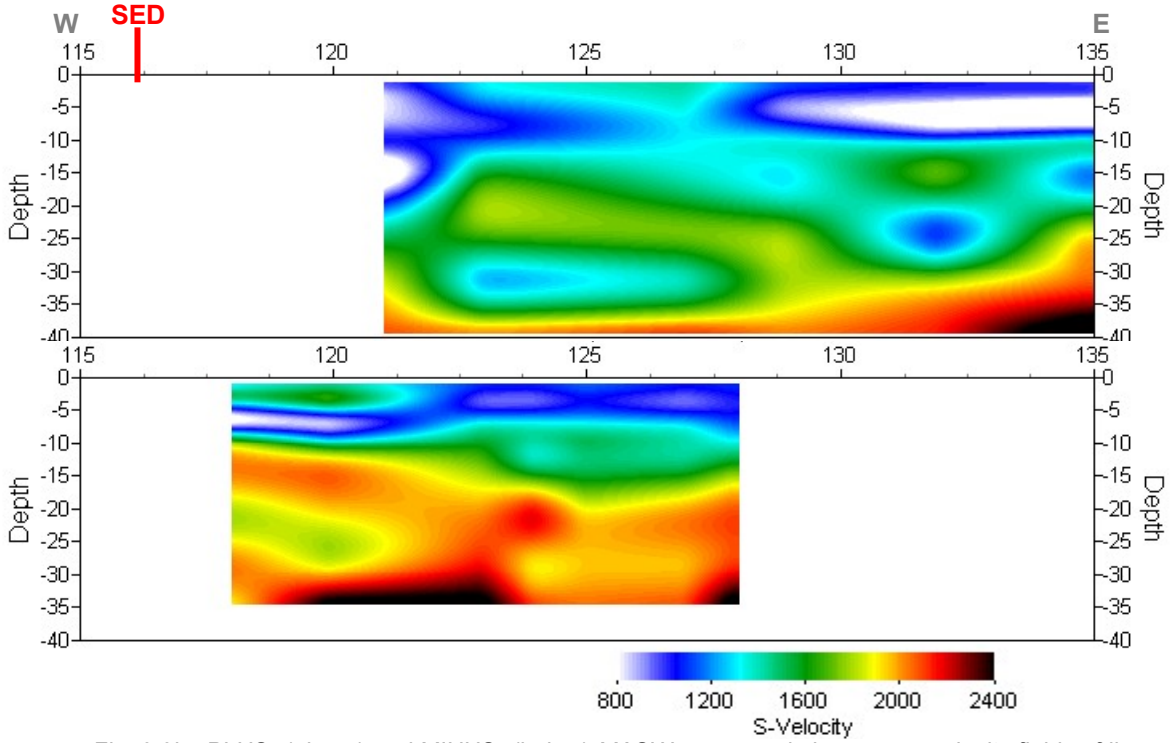

Fig. 3.3h: PLUS- (above) and MINUS- (below)-MASW-processed shear wave velocity fields of line 09SN_20WIMIS-M1. Profile station number 101 = profile meter 0, profile station 148 = profile meter 172; station spacing is 1.5

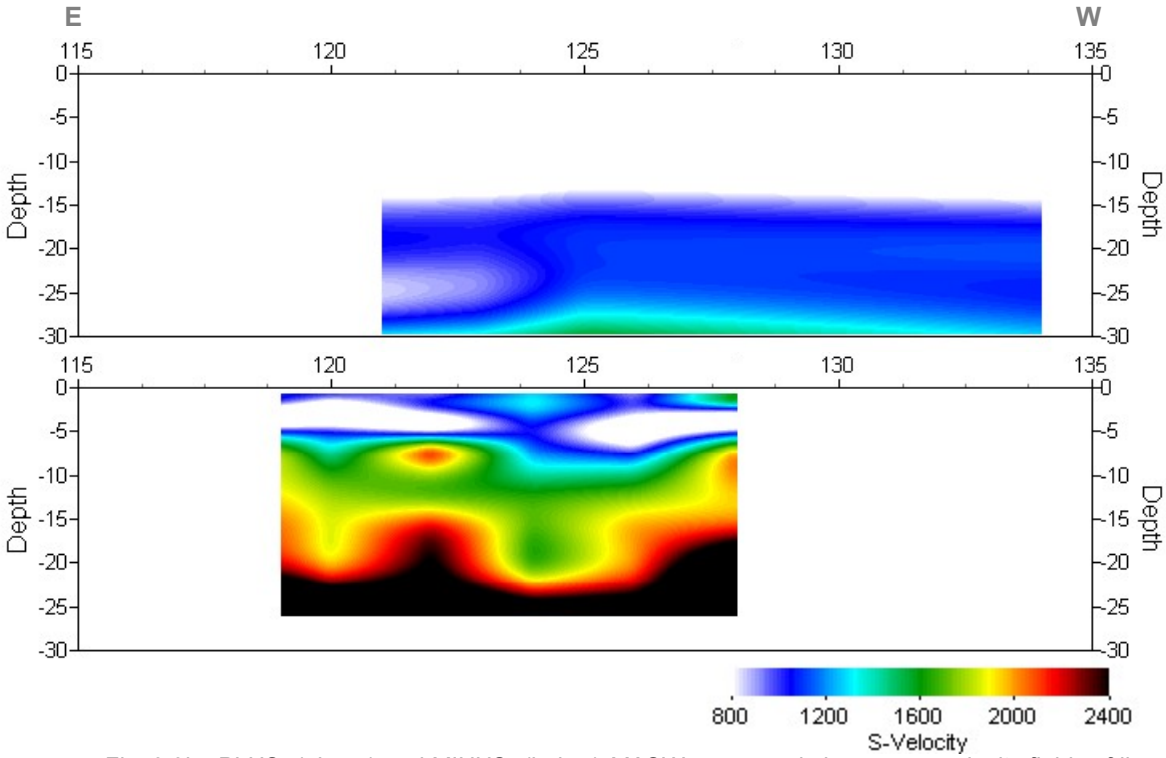

Fig. 3.3i: PLUS- (above) and MINUS- (below)-MASW-processed shear wave velocity fields of line 09SN_20WIMIS-M2. Profile station number 101 = profile meter 0, profile station 148 = profile meter 172; station spacing is 1.5 m.

3.3.6 Calculation of the average shear wave velocity

In order to calculate a representative shear wave velocity-depth function of line 09SN_20WIMIS-M1 at the SED station, all computed 1D-v_S-depth functions are averaged (non-weighted mean values). The v_S-depth-function is shown in Tab. 3.3a.

Depth [m]	Vs+ [m/s]	Vs- [m/s]	Vs [m/s]
1.2	1167	1149	1158
2.6	1188	1106	1147
4.4	1099	890	994
6.7	1099	949	1024
9.5	1387	1249	1318
13.1	1624	1274	1449
17.5	1853	1400	1627
23.0	2004	1620	1812
29.9	1993	1699	1846
37.4	2249	2214	2231

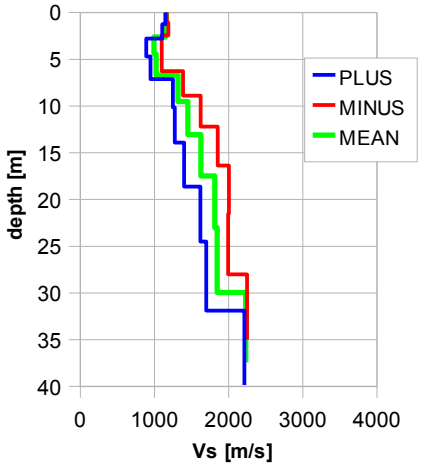

Tab. 3.3a: Averaged vs - depth function of line 09SN_20WIMIS-M1 at the SED station WIMIS. Blue line: MASW-'PLUS' processing, red line: MASW-'MINUS' processing; green line: average of PLUS- and MINUS-functions.

In order to calculate an representative shear wave velocity-depth function of line 09SN_20WIMIS-M2 at the SED station, all computed 1D-v_S-depth functions are averaged (non-weighted mean values). The resulting v_S-depth-function is shown in Tab. 3.3b.

Depth [m]	Vs- [m/s]	Vs+ [m/s]	Vs [m/s]
0.9	1105	552	829
2.0	1173	504	838
3.5	761	560	660
5.2	800	516	658
7.5	1407	509	958
10.2	1685	571	1128
13.7	1777	910	1343
18.0	1991	1076	1534
23.5	2292	1012	1652
29.3	3200	1636	2418

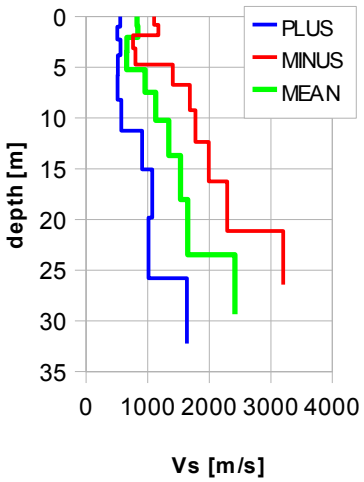

Tab. 3.3b: Averaged v_S - depth function of line 09SN_20WIMIS-M2 at the SED station WIMIS. Blue line: MASW-'PLUS' processing, red line: MASW-'MINUS' processing; green line: average of PLUS- and MINUS-functions.

The inversion of the four 70 m-array dispersion curves data (10 to 80 m offset, see Fig. 3.3f and 3.3g) are given in Tab. 3.3c. These values are complemented with the values derived of the 40 m-arrays analyses (Tab. 3.3a and 3.3b).

70 m array								40 m array			
depth	m1+	depth	m1-	depth	m2+	depth	m2-	depth	m1	depth	m2
1.8	1617	0.8	1316	1.2	1286	1.1	1590	1.2	1158	0.9	829
4.1	1613	1.9	1312	2.7	1203	2.4	1670	2.6	1147	2.0	838
6.9	1583	3.2	1216	4.6	1119	4.2	1533	4.4	994	3.5	660
10.4	1521	4.8	1219	7.0	1214	6.3	1268	6.7	1024	5.2	658
14.8	1468	6.9	1331	10.0	1301	8.9	1537	9.5	1318	7.5	958
20.3	1584	9.4	1365	13.7	1496	12.3	2044	13.1	1449	10.2	1128
27.2	1995	12.6	1216	18.3	2057	16.4	2301	17.5	1627	13.7	1343
35.8	2359	16.6	1141	24.1	2350	21.6	2422	23.0	1812	18.0	1534
46.6	2248	21.6	1795	31.4	1772	28.1	2558	29.9	1846	23.5	1652
58.2	2058	27.0	1718	39.3	2645	35.1	2883	37.4	2231	29.3	2418

Tab. 3.3c: v_s-depth values of the four MASW-derived dispersion curves of both seismic line 09SN_20WIMIS-M1 and 09SN_20WIMIS-M2 using 70 m-arrays. The dispersion curves are shown in Fig. 3.3f and Fig 3.3g.

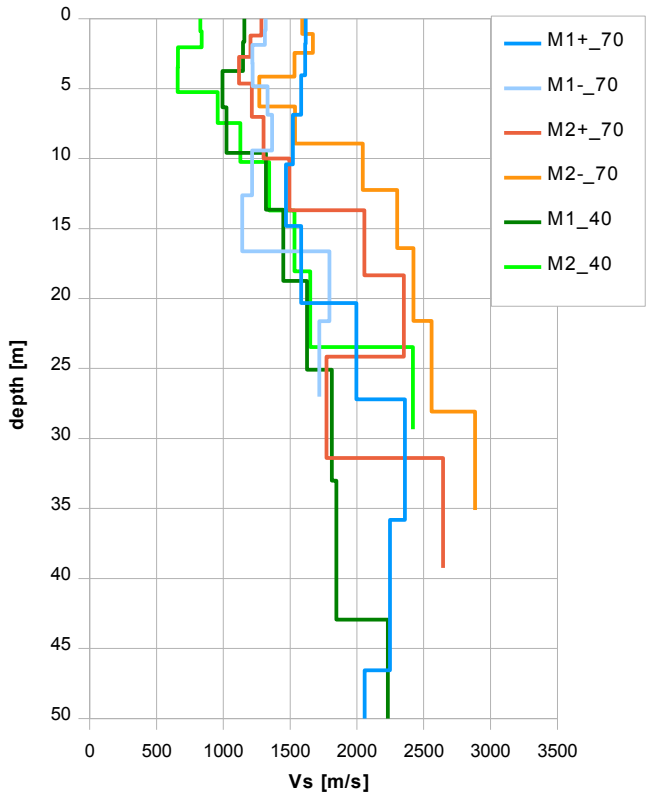

Fig. 3.3j: Comparison of the ensemble of inversion results of both lines 09SN_20WIMIS-M1 and -M2, either using the 40 m- and the 70 m-arrays.
blue lines: analyses of records of line 09SN_20WIMIS-M1, 70 m arrays
red lines: analyses of records of line 09SN_20WIMIS-M2, 70 m arrays
green lines: v_s-values of analyses of 40 m array records.

3.3.7 Calculation of the shear wave velocity scalars $v_{s,5}$, $v_{s,10}$, ...

The parameters $v_{s,5}$, $v_{s,10}$, $v_{s,20}$, $v_{s,30}$, $v_{s,40}$, $v_{s,50}$ represent the average shear wave velocities in the depth interval between the surface and the respective depth levels and are determined from the formula

$$v_{s,n} = \frac{\sum_{i=1}^{n} d_i}{\sum_{i=1}^{n} d_i / v_{si}}$$

with:

d_i = thickness of layer i

v_{si} = corresponding shear-wave velocity.

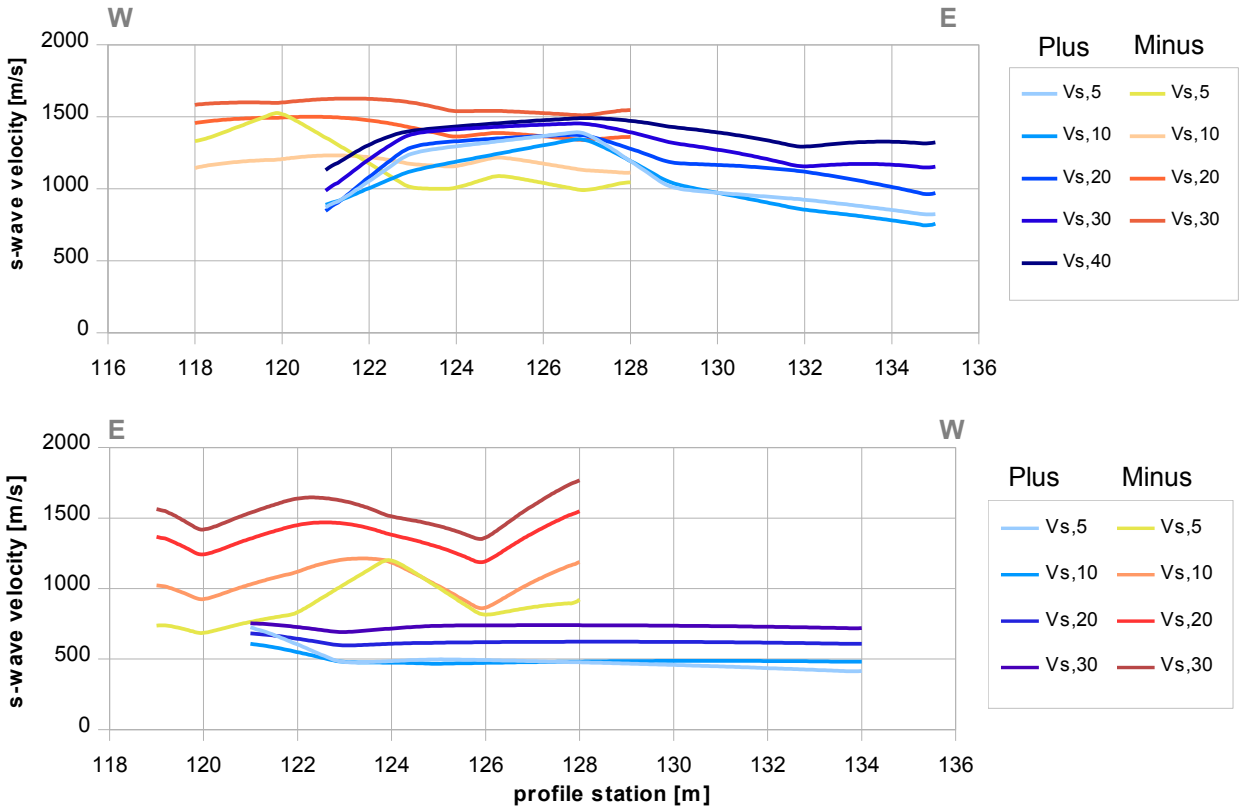

Fig. 3.3l: Graphs of the averaged $v_{s,5}$...-values along the line 09SN_20WIMIS-M2 for the PLUS- (blue lines) and MINUS- (red lines) directions.

The average values of the s-wave velocity model $v_{s,5}$, $v_{s,10}$, $v_{s,20}$, $v_{s,30}$, $v_{s,40}$, $v_{s,50}$, $v_{s,100}$ (= average shear wave velocity from the surface to depths of 5 m, …until 50 m) on the line segment nearest to the SED station (Tab. 3.3d) are summarized below:

M1	Vs,5	Vs,10	Vs,20	Vs,30	Vs,40
MINUS	1181	1183	1425	1573	n/a
PLUS	1092	1042	1190	1292	1384
MEAN	1137	1112	1308	1433	1384

M2	Vs,5	Vs,10	Vs,20	Vs,30	Vs,40
MINUS	892	1057	1360	1534	n/a
PLUS	486	491	621	730	n/a
MEAN	689	774	990	1132	n/a

Tab. 3.3d: The average shear wave velocities within the depth intervals from surface down to 5 m, etc.… to 40 m of line 09SN_20WIMIS-M1 (top) resp. of line 09SN_20WIMIS-M2 (bottom).

3.4 Hybrid Seismic Data Processing

3.4.1 p-wave *Reflection* Seismic Processing Sequence

A) Data conditioning

A1 Reformatting and quality verification of field data
A2 Recording geometry assignment
A3 Data editing (suppression of bad / dead traces, etc.)
A4 Preliminary analysis of refraction velocities

B Filtering and deconvolution

B1 Analytical muting of refraction arrivals
B2 Amplitude recovery / amplitude equalization in time and frequency domains
B3 Predictive deconvolution parameter tests / application
B4 Determination of band limiting corner frequencies / application
B5 Optional 2-D filtering

C) Velocity analysis and stack

C1 Common Depth Point (CDP) sort
C2 Semblance velocity analysis using supergathers of 3 - 5 CDP's
C3 Optional dip move-out correction
C4 Normal Move-Out (NMO) correction and application of stretch mute
C5 Band-pass filtering
C6 CDP stack
C7 Optional coherency filtering

D) Time-depth conversion

D1 Optional spiking deconvolution
D2 Band-pass filtering
D3 Depth conversion
D4 Final display of seismic depth section with inversed polarity (non-SEG-convention)

3.4.2 The presentation of reflection seismic data

The reflection seismic processing of the p-wave dataset does not give any useful result for lack of reflection events in the nearly homogeneous limestone.

3.4.3 p-wave refraction tomography processing

The seismic p-wave refraction processing steps are analogous to those described in paragraph 3.2. For a detailed method statement and a description of the processing steps please refer to the summary report. The Figs. 3.4d to 3.4i and Tab. 3.4a illustrate the intermediate processing steps and the final result.

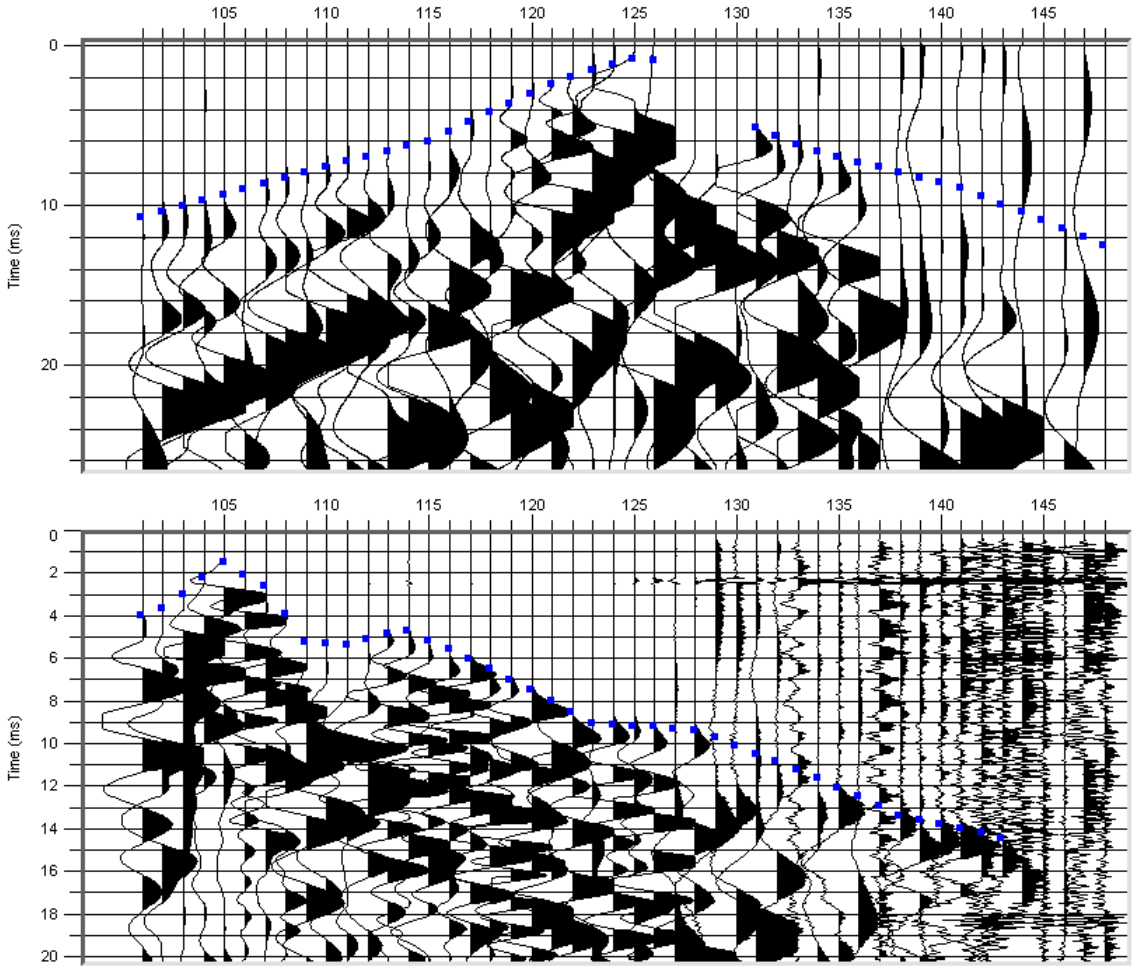

Fig. 3.4d: p-wave records of 09SN_20WIMIS-P1 (top) and -P2 (bottom) with positive amplitude excursions in black. Colored dots mark the manually picked first break arrival times. Vertical axis: travel time in ms, horizontal axis: station numbers spaced at 1.5 m.

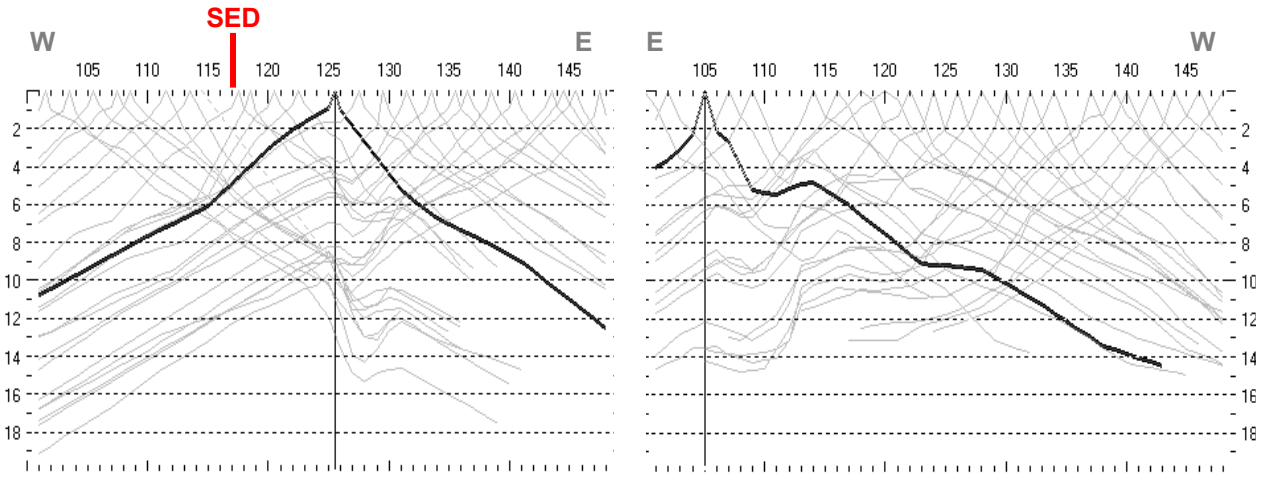

Fig. 3.4e: Travel time curves of p-wave arrival time picks of line 09SN_20WIMIS-P1 (left) and -P2 (right). Vertical axes: travel time [ms], horizontal axes: station number. Profile station 101 = profile meter 0; profile station 148 = profile meter 172.

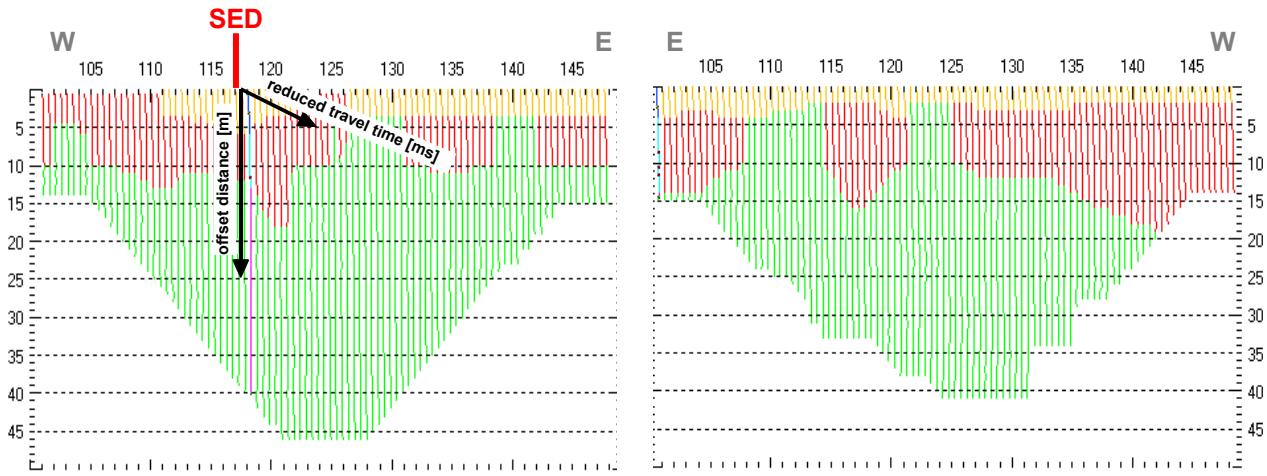

Fig. 3.4f: 3-dimensional distance-travel time diagrams at the mid-points between source points and receiver stations are instrumental when using the analytical CMP derivation of the initial velocity field. The horizontal axes are along the CMP positions and the travel time respectively, the vertical axis denotes the offset distance between source and receiver positions.

Depth [m]	Vp [m/s]
0.0	817
0.2	1443
0.3	1864
0.7	2107
1.1	2348
1.7	2729
2.5	3152
3.7	3601
5.2	3781
7.4	4511
10.5	4977
14.8	5000

Depth [m]	Vp [m/s]
0.0	1054
0.3	1441
0.5	1672
0.9	1931
1.5	2268
2.4	2834
3.5	3424
5.1	4108
7.3	4825
10.5	5242
14.9	5846
21.0	5869
29.7	5869

Tab. 3.4a: Initial 1D p-wave velocity model derived from real data (left: 09SN_20WIMIS-P1; right: -P2).

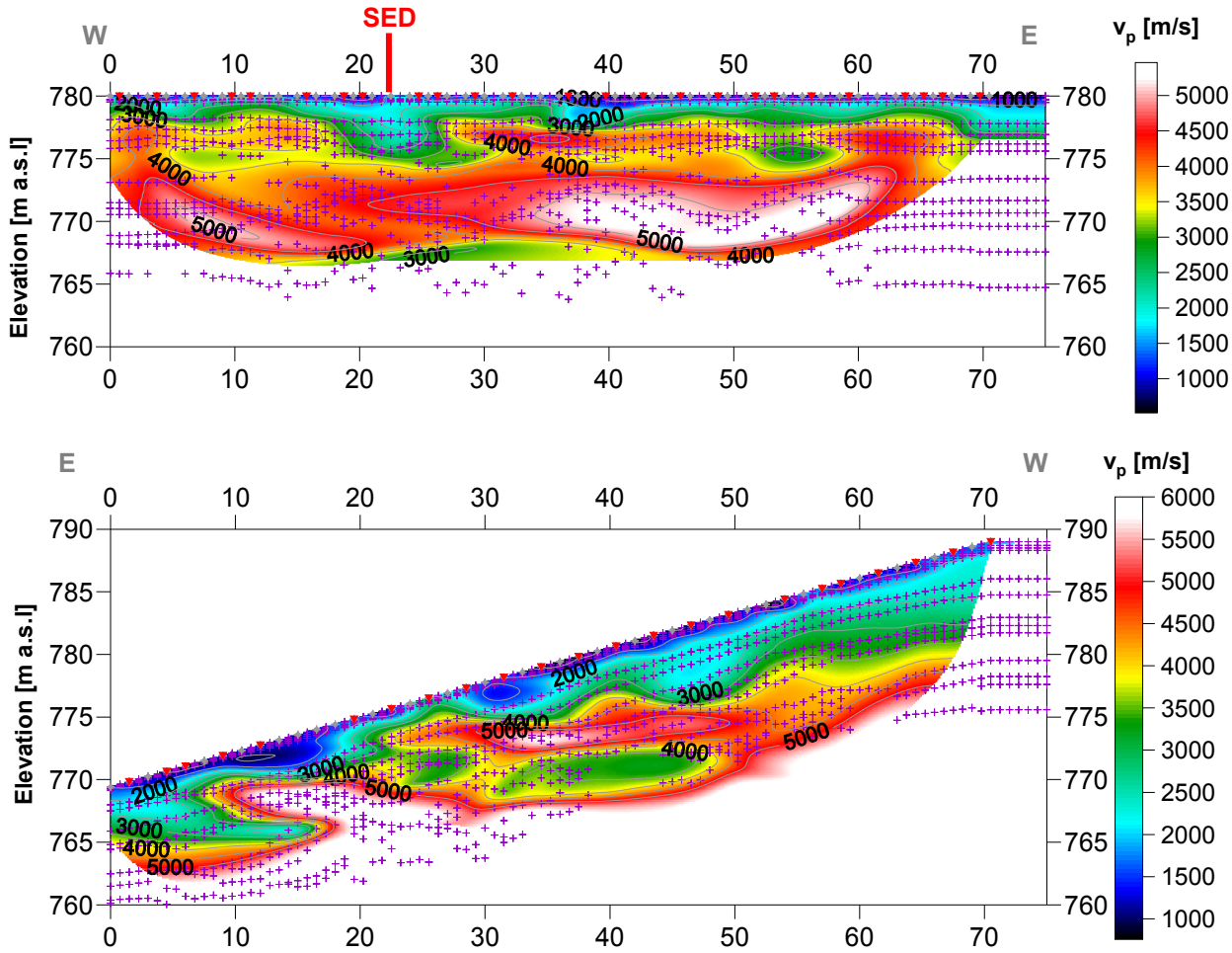

Fig. 3.4g: Compressional wave velocity field image along the seismic profiles 09SN-20WIMIS-P1 (above) and -P2 (below). Red/white colors indicate solid rock, blue/black colors unconsolidated sediments and soil. Vertical axis: elevation [m a.s.l]; horizontal axis: profile meter; color scale: v_s [m/s]; no vertical exaggeration; gray squares: receiver stations; red triangles: shot positions; magenta crosses: positions of determined velocity values. The station spacing is 1.5 m, profile meter 0 = profile station number 101, profile meter 72 = profile station number 148.

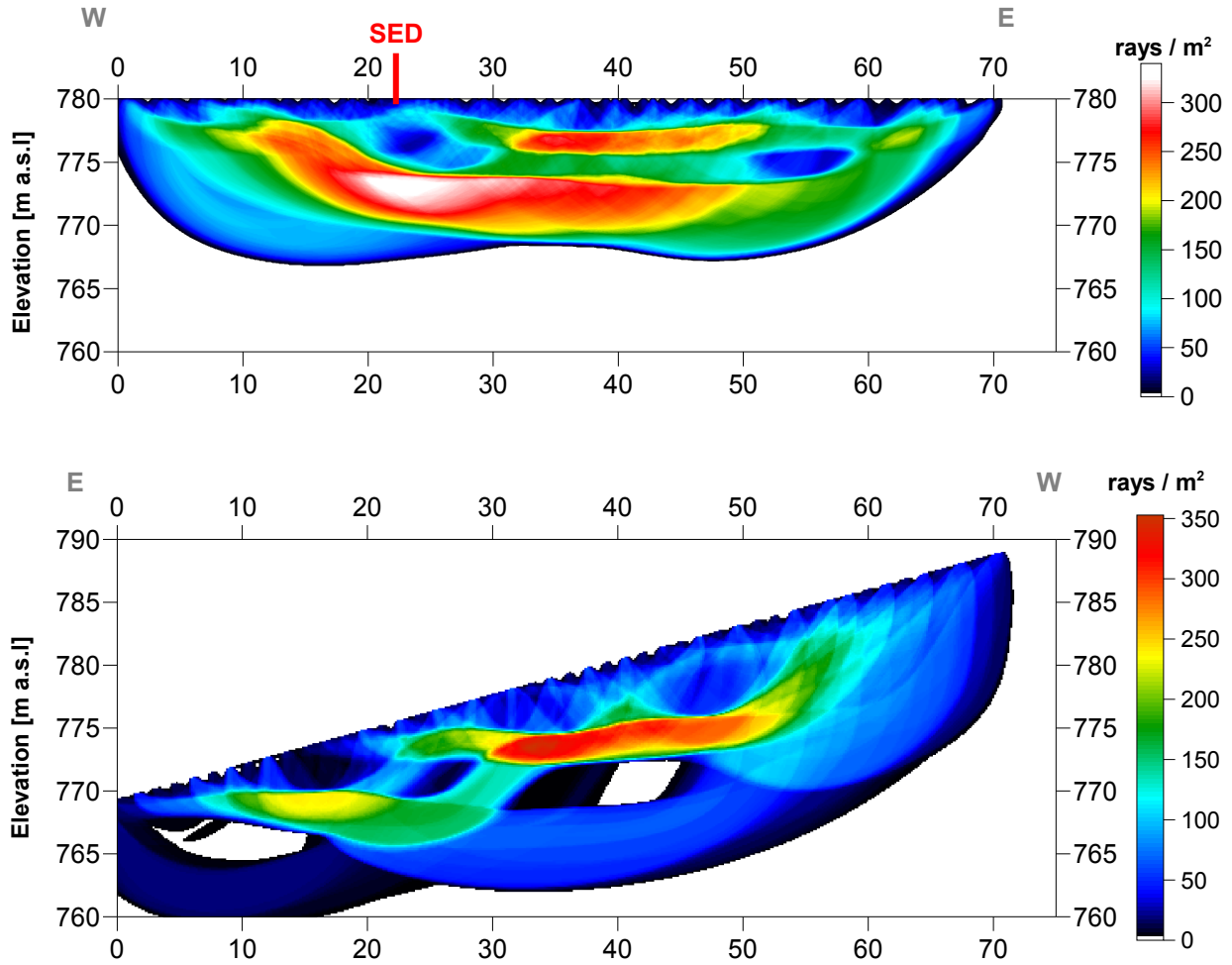

Fig. 3.4h Compressional wave subsurface ray path density along the seismic profiles 09SN_20WIMIS-P1 (above) and -P2 (below). Red/white colors indicate high velocity contrast between two layers, blue/black colors low coverage areas. Vertical axis: elevation [m a.s.l]; horizontal axis: profile meter; color scale: ray paths per m2; no vertical exaggeration.
The station spacing is 1.5 m, profile meter 0 = profile station number 101, profile meter 72 = profile station number 148.

Depth [m]	Vp [m/s]
0.0	1089
0.9	2045
1.6	2581
2.4	3347
3.2	3372
4.0	3044
4.8	3104
5.5	3341
6.3	3981
7.1	4706
7.9	4755
8.7	4589
9.4	4151
10.2	4339
11.0	4615
11.8	4855
12.6	5082

Depth [m]	Vp [m/s]
0.0	1355
0.8	1715
1.6	2251
2.4	2661
3.2	3032
4.0	3413
4.8	3730
5.6	3968
6.4	4124
7.2	4260
8.0	4393
8.8	4597
9.6	4653
10.4	4547
11.2	4663
12.0	5045
12.8	5405
13.6	5663
14.4	5886

Tab. 3.4b: Final 1D p-wave velocity model derived from real data at line 09SN_20WIMIS-P1 (left) resp. at line -P2 (right) .

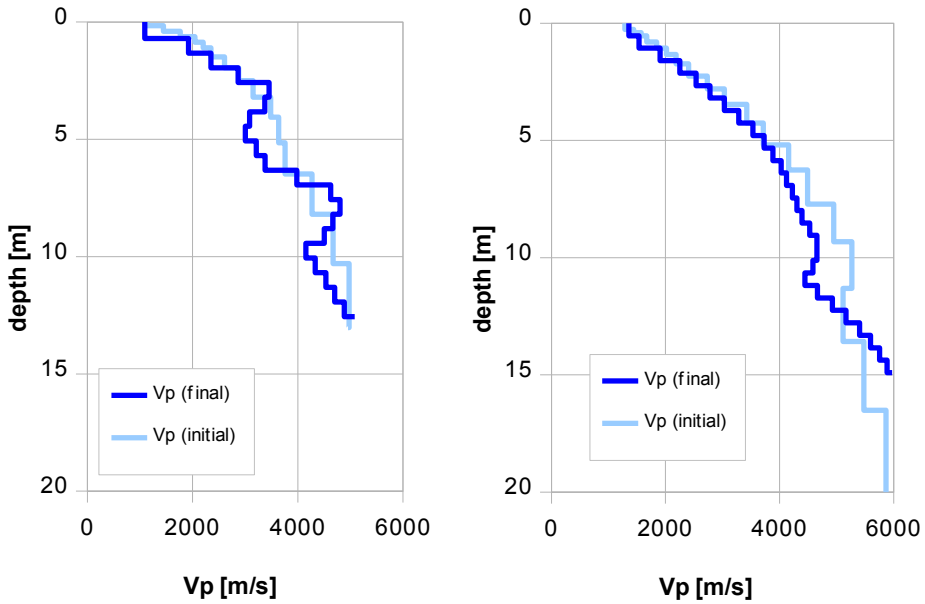

Fig. 3.4i: Final 1D p-wave velocity model derived from real data at line 09SN_20WIMIS-P1 (left) resp. at line -P2 (right). Initial 1D p-wave velocity model values are given in Tab. 3.4a.

4 DISCUSSION OF THE RESULTS

4.1 Summary and Validation of the Results

Compressional and shear wave velocity data from refraction seismic surveys both p-wave and s-wave and also the MASW survey data of profiles 09SN_20WIMIS-1 and 09SN_20WIMIS-2 are shown in Tab. 4.1 for the uppermost 30 m. The calculated shear wave velocity $v_{s(calc)}$ in Tab. 4.1 is derived by using a theoretical v_p/v_s-ratio of $\sqrt{3}$.

Depth	Vp1	Vp2	Vs1	Vs1	Vs2	Vs2	Vs1	Vs2
	meas	meas	meas	calc	meas	calc	MASW	MASW
0	1089	1355	870	629	536	782	1158	829
1			1183		803		1147	838
2	2346	1904	1373	1355	1010	1100		660
3	2867	2535	1349	1655	1324	1464	994	658
4	3372	3032	1419	1947	1409	1750	1024	
5	3000	3532	1536	1732	1597	2039		958
6	3209	3885	1570	1853	1695	2243		
7	3981	4124	1498	2298	1854	2381	1318	1128
8	4625	4306	1483	2670	1910	2486		
9	4663	4393	1455	2692	1824	2536		
10	4151	4654	1427	2396	1817	2687	1449	1343
11	4330	4588	1504	2500	1772	2649		
12	4702	4663	1840	2715	1769	2692		
13	4885	5167	1878	2820	1797	2983	1627	
14		5598			1885	3232		1534
15		5886			1940	3398		
16					2090			
17					2177		1812	
18					2364			1652
19								
20								
21								
22								
23							1846	2418
24								
25								
26								
27								
28								
29								
30							2231	

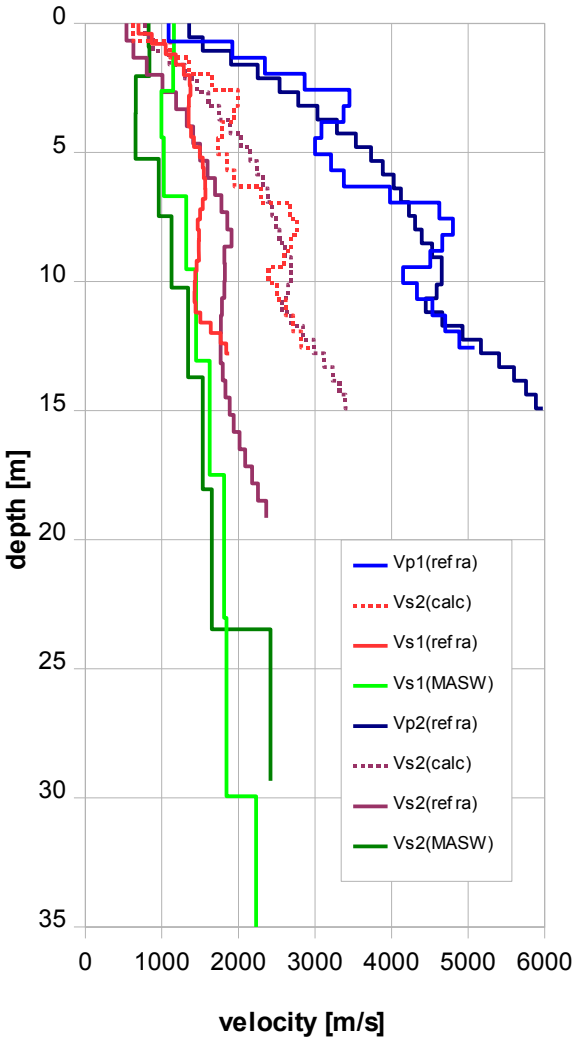

Tab. 4.1: Shear and compressional wave velocity model determined at the SED station WIMIS.

Fig. 4.1: Graphic display of measured (continuous lines) and calculated (dotted lines) wave velocities at the SED station. In blue colors values of p-wave dataset, in red colors of s-wave datases and in green colors values of MASW analyses.

4.2 Validation of the methods and their results

Due to methodological differences, v_s velocities derived by MASW analysis and by the refraction tomography technique may differ considerably. This is because MASW analysis cannot image small rock/soil inhomogeneities as a dispersion image with an array length of i.e. 40-m only yields one single v_s-value at each depth. On the other hand, refraction diving wave tomography results produce v_s-sections with a high lateral resolution, but fail to provide information at greater depths.

4.3 Error Estimates

The error estimates given in Tab. 4.3 below are relevant only in the context of this survey.

Surveying method	Type of result	Error estimate
v_s – refraction tomography	v_s – velocity field image	15%
MASW only "+" or only "-" values	v_s – velocity field image	20%
MASW (mean of "+" & "-" values)	v_s – velocity field image	15%
v_p – refraction tomography	v_p – velocity field image	10%

Tab. 4.3 Error estimates for the methods applied. Note that higher error estimates are to be taken into account with increasing depths.

The above error estimates are of a qualitative character only. A handicap in both MASW and refraction tomography was that large velocity contrasts in the uppermost half a meter along the profiling. So interrupt considerably the two bunker entrances along line 09SN_20WIMIS-1 (profile meter 22 (where the SED monitoring station is located in) and 38) the wave field. This leads to nonlinear surface waves and non-linear refraction first breaks. On line 09SN_20WIMIS-2, tectonic faults resp. layerings with weathered contacts of 0.5 to 4 m width disturbed the data as well.

Nevertheless, all velocity data coincide well, independently of the methodological differences, the MASW values are generally 10 – 30 percent lower than refraction tomography values.

5 SUMMARY AND CONCLUSIONS

- In April 2009 a combined seismic s- and p-wave survey was carried out at the SED earthquake monitoring station WIMIS near Wimmis BE.
- The wave generation was conducted directly onto the solid rock where possible. So are the horizontal and vertical geophones planted in direct contact with the rock where possible.
- The shear wave data have been evaluated by conventional diving wave refraction tomography techniques in order to derive the s-wave velocity field along the seismic line. Due to the inherent constraints of the refraction tomography method, the depth of investigation is limited to 12 m under the prevailing geological conditions.
- The p-wave data have been processed
  - firstly to derive a 2D s-wave velocity field by using the MASW (**M**ultichannel **A**nalysis of **S**urface **W**aves) technique;
  - and secondly, according to the hybrid seismic data processing scheme for representing the subsurface structures in a combined reflection seismic section with the superimposed p-wave velocity field.
- The shear wave velocity range determined by the MASW method in the uppermost 30 meters spans from values of 658 m/s to 2418 m/s.
- The scalar values derived by the MASW survey at the SED station (seismic line 09SN_20WIMIS-M1, profile station 55; seismic line 09SN_20WIMIS-M2, profile station 45) are the following:

line 1			line 2		
$v_{s,5}$	=	1137 m/s	$v_{s,5}$	=	689 m/s
$v_{s,10}$	=	1112 m/s	$v_{s,10}$	=	774 m/s
$v_{s,20}$	=	1308 m/s	$v_{s,20}$	=	990 m/s
$v_{s,30}$	=	1433 m/s	$v_{s,30}$	=	1132 m/s
$v_{s,40}$	=	1384 m/s	$v_{s,40}$	=	n/a

- The estimated reliable refraction shear wave velocity of hard rock is 1750 m/s.
- The estimated reliable refraction compressional wave velocity of hard rock is 4300 m/s
- The geophysical interpretation of the subsurface structures in this report are to be validated and incorporated into a comprehensive appraisal by a geologist familiar with the local geological setting.

Schwerzenbach, 8th July 2009

Walter Frei
dipl. Natw. ETH
managing director

Lorenz Keller
dipl. Natw. ETH
project manager